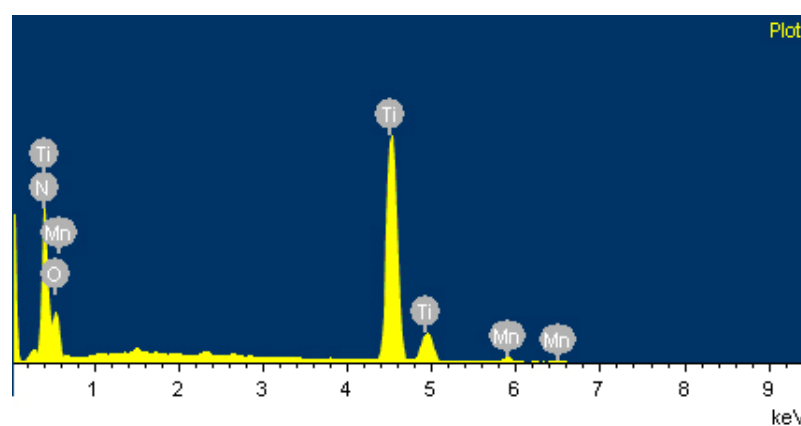


Supporting Information (SI) for Coaxial MnO₂/Titanium Nitride Nanotube Arrays for High-rate Electrochemical Capacitive Energy Storage

Shanmu Dong, Xiao Chen, Lin Gu, Lanfeng Li, Xinhong Zhou, Zhihong Liu,
Pengxian Han, Hongxia Xu, Jianhua Yao, Haibo Wang, Xiaoying Zhang, Chaoqun
Shang, Guanglei Cui ^{*}, Liquan Chen

Figure S1. EDS pattern of mesoporous MnO₂ deposited on TiN at deposition potential of 0.7 V for 10 s.

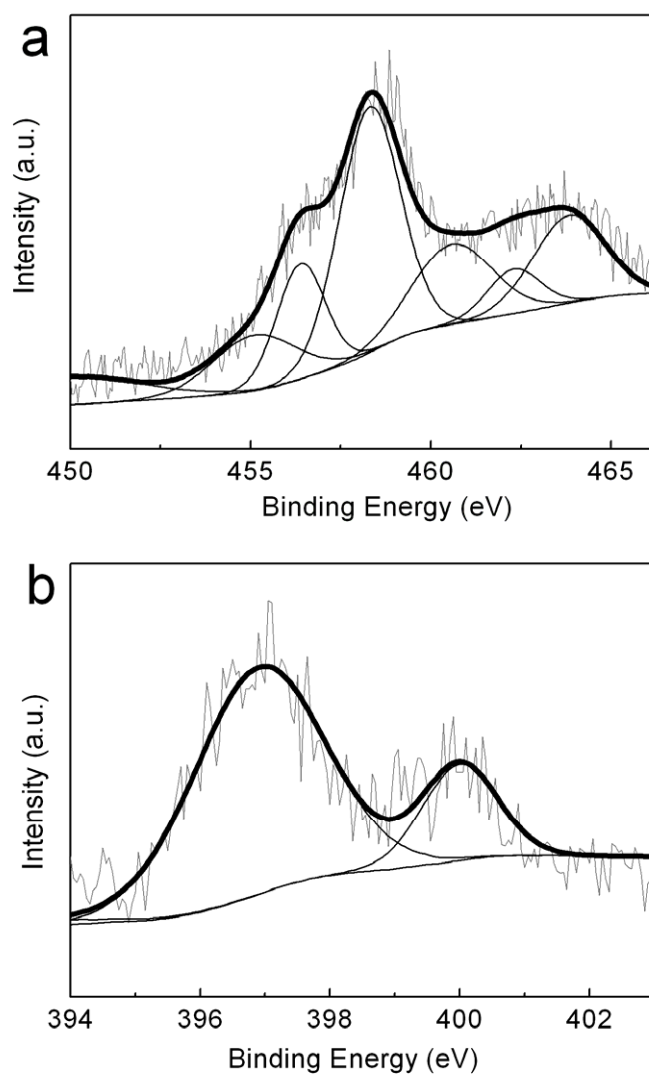


S2. XPS study

Figure S2 (a) displays the Ti 2p deconvoluted bands for as prepared coaxial MnO₂/TiN NTA. The Ti 2p_{3/2} line is at the binding energies of 455.1 eV, 456.5 eV, and 458.3 eV for TiN, TiO_xN_y, and TiO₂, respectively.¹⁻² Figure S2 (b) shows the N 1s line with a major peak of 396.9 eV for TiN and TiO_xN_y.¹ The presence of TiO₂ and TiO_xN_y can be attributed to the surface passivation of TiN with atmospheric oxygen. Furthermore, these results confirm the presence of TiN in the nanostructured

composite materials.

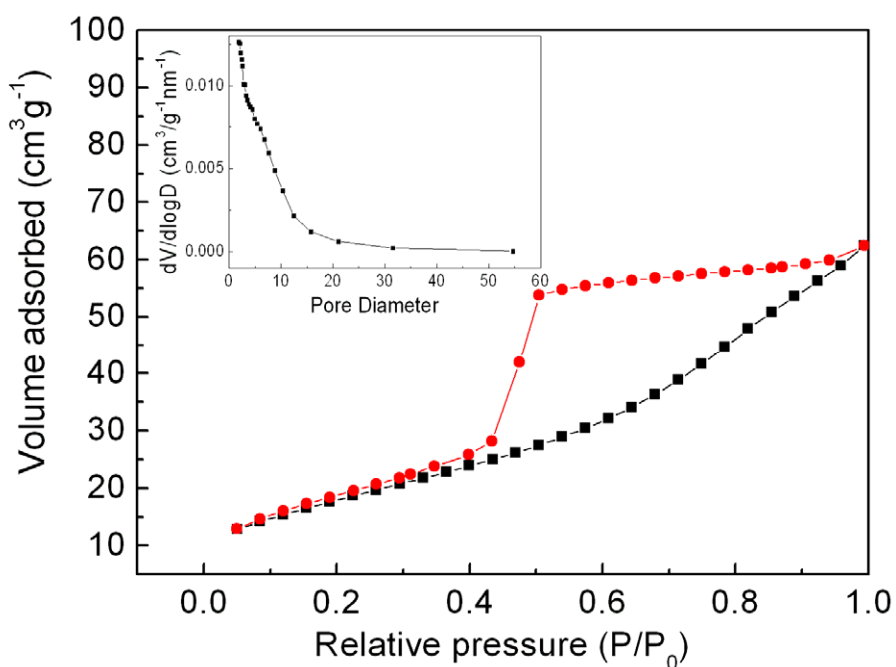
Figure S2. XPS spectra for the coaxial MnO₂/TiN NTA samples in the region of binding energies of Ti 2p and N 1s



S3. The N₂ adsorption-desorption analysis of electrodeposited MnO₂

The porosity of the electrodeposited MnO₂ materials is determined by nitrogen sorption measurement (Figure S2 Supporting Information). The N₂ adsorption-desorption isotherms of the material are identified as Type IV isotherm indicating characteristics of mesoporous materials. The surface area, pore volume, and average pore size were 66.0 m² g⁻¹, 0.10 cm³ g⁻¹, and 5.60 nm, correspondingly.

Figure S3. Nitrogen adsorption and desorption isotherms of electrodeposited MnO_2 and their pore-size distribution (inset) obtained from adsorption branch of the isotherm using the BJH method.



S4. The formation of MnO_2/TiN NTA with “hollow structure”

The growth process of MnO_2/TiN NTA with “hollow structure” is briefly suggested as follows: during the deposition under higher potential, Mn^{2+} inside the nanotube was quickly depleted, resulting in a higher concentration of Mn^{2+} at the top surface than that at the bottom of nanotubes. Consequently, a faster formation of MnO_2 layer at the nozzle will further block the transport of Mn^{2+} into the inner of the tubes.

Figure S4. Low and high magnification (inset) SEM images of MnO₂/TiN NTA with “hollow structure” formed at deposition potential of 0.9 V for 10 s (mechanically fractured).

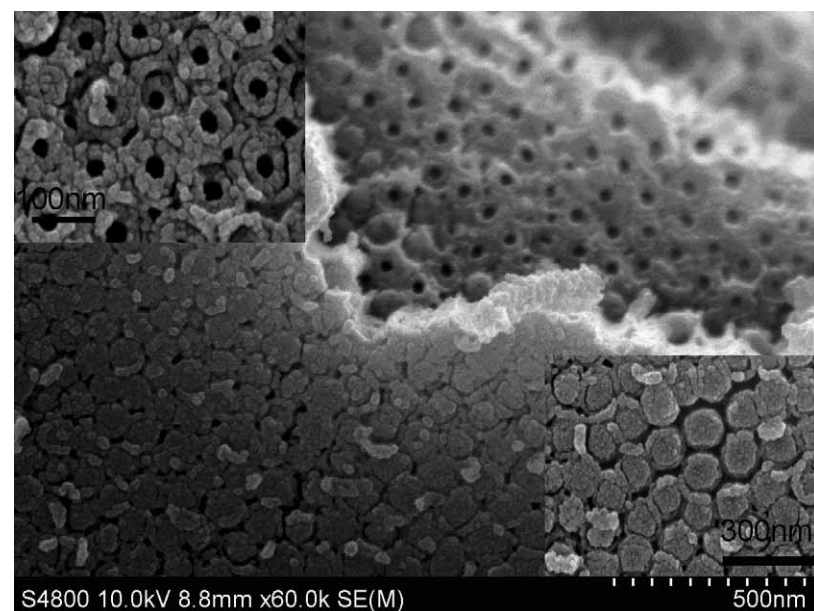
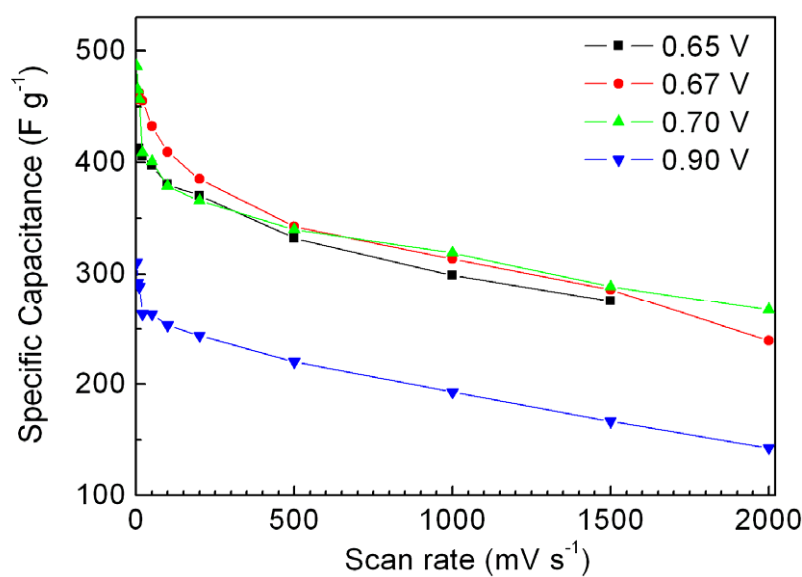


Figure S5. Specific capacitance (F g^{-1}) of MnO₂/TiN NTA electrodes (based on the mass of MnO₂) obtained at different applied potential as a function of scan rates.



S6 Simulation of EIS data

An equivalent circuit was used to analyze the measured impedance data (Figure 5d),³⁻⁵ where R_s includes the bulk electrolyte solution resistance and the intrinsic resistance of active material, R_{ct} represents the kinetic resistance to charge transfer at electrode–electrolyte interface, W associates with the semi-infinite diffusion of cation in the bulk electrode, CPE used in place of double-layer capacitance and C is used in place of pseudocapacitance. As shown in Figure 5d, the calculated Nyquist plots overlaps with the measured ones well, as the χ^2 value between the fitted and the experimental plots of MnO_2/TiN NTA and MnO_2/TiN thin film were 3.87×10^{-4} and 1.03×10^{-3} , respectively.

Table S6 Values of the equivalent circuit components used for fitting the EIS experimental curve of MnO_2/TiN NTA and MnO_2/TiN thin film.

component	Fitted values	
	MnO_2/TiN NTA	MnO_2/TiN thin film
R_s (Ω)	3.4	3.6
R_{ct} (Ω)	1.1	8.3
CPE (S s^{-n})	0.0014	0.00070
n	0.73	0.64
W ($\text{S s}^{1/2}$)	0.087	0.012
C (F)	0.0045	0.0026

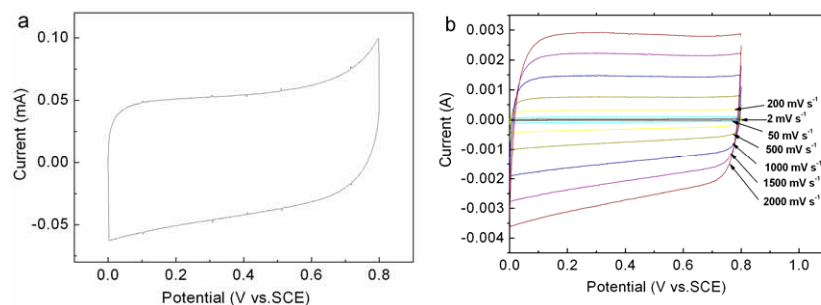
S7. Calculations

For the supercapacitors application, according to the literature reported by Lee et al.,⁶ the mass of the electrodeposited MnO_2 can be calculated from the charge passed for the electrochemical deposition based on Faraday's laws of electrolysis. In a typical process, the electrochemical deposition was carried out at 0.7V for 10 s to give a totally passed charge of 40 mC at TiN NTA electrode with 0.25 cm^2 . The calculated

mass of MnO_2 is about 0.06 mg cm^{-2} .

As the TiN NTA is directly grown from Ti foil substrate, it is hard to obtain the mass of TiN NTA accurately. Therefore, the TiN NTA was carefully peeled off using a doctor blade and weighed on precision balance (METTLER TOLEDO XS105). Then the fractured film was grinded into powder to mix with 5 % super P and 10 wt % PTFE binders. The samples were then cut into plates of $0.5 \text{ cm} \times 0.5 \text{ cm}$ and pasted on a stainless steel current-collector under a pressure of 15 MPa to fabricate a electrode of TiN. We have to assume that the specific capacity calculated from CV cuve of TiN electrode is the same as that of the TiN NTA on the Ti foil substrate at a low scan rate. As calculated from Figure S6 (a), the specific capacity of TiN electrode is 21.3 F g^{-1} at the scan rate of 2 mVs^{-1} . Therefore the mass of TiN NTA on Ti foil substrate with 0.25 cm^2 (according to Fig S6b) was approximately 0.11 mg , correspondingly. Consequently, the specific capacity of overall MnO_2/TiN electrode is roughly 80 F g^{-1} at the scan rate of 2 mVs^{-1} .

Figure S7. (a) The CV curve of TiN electrode at the the scan rate of 2 mVs^{-1} . (b) The rate-dependent CV curves of TiN NTA on Ti foil substrate at various scan rates from 2 to 2000 mVs^{-1} .



References

- 1 M. Zukalova, J. Prochazka, Z. Bastl, J. Duchoslav, L. Rubacek, D. Havlicek, L. Kavan, Chem. Mater., 2010, **22**, 4045.
- 2 M. Drygas, C. Czosnek, R. T. Paine, J. F. Janik, Chem. Mater. 2006, **18**, 3122.
- 3 C. Xu, H. Du, B. Li, F. Kang, Y. Zeng, J. Electrochem. Soc., 2009, **156**, A73-A78.
- 4 J. Rishpon, S. Gottesfield, J. Electrochem. Soc., 1984, **131**, 1960.
- 5 S. Devaraj, N. Munichandraiah, J. Electrochem. Soc., 2007, **154**, A808.
- 6 R. Liu, S. B. Lee, J. Am. Chem. Soc., 2008, **130**, 2942-2943.